Journal of Power Sources 257 (2014) 264–271

Contents lists available at ScienceDirect

Journal of Power Sources

journal homepage: www.elsevier.com/locate/jpowsour

Effect of different trap states on the electron transport of photoanodes in dye sensitized solar cells

Jing Zhang [a,*], Jiangwei Feng [a], Yang Hong [a], Yuejin Zhu [a,**], Liyuan Han [b,**]

[a] Department of Physics, Ningbo University, Zhejiang 315211, China
[b] Photovoltaics Materials Unit, National Institute for Materials Science, Tsukuba, Ibaraki 305-0047, Japan

HIGHLIGHTS

- Surface traps and bulk traps in the photoanodes of DSSCs are distinguished in this work.
- The influence of each trap state to the electron transport is characterized.
- Bulk trap states should be avoided during photoanode preparation to get high quality DSSCs.
- Interface recombination time is closely related to the property of the trap states.

GRAPHICAL ABSTRACT

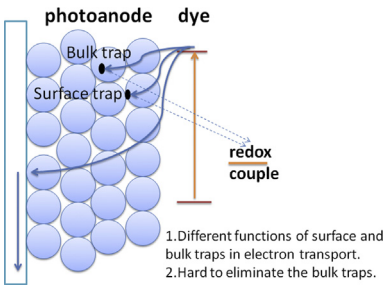

ARTICLE INFO

Article history:
Received 14 November 2013
Received in revised form
27 December 2013
Accepted 17 January 2014
Available online 7 February 2014

Keywords:
Dye sensitized solar cells
Doping of semiconductor
Surface traps
Bulk traps
Electron transport

ABSTRACT

Trap states play important role in electron transport of dye sensitized solar cells (DSSCs). Different trap states (surface and bulk traps) contribute differently to the performance of DSSCs. However, there is a lack of classification of the trap states, especially in recent doping works of the photoanodes. In this work, the Ce^{4+} (0.3, 0.6 and 0.9% molar ratio) in TiO_2 and Ti^{4+} (15, 40 and 70% molar ratio) in SnO_2 are assigned to surface traps and surface-and-bulk coexisted traps, respectively. The property of each trap state and its influence to the electron transport are characterized. Both the surface and bulk traps deteriorate the electron transport in DSSCs, however, the negative role of surface traps can easily be eliminated by surface modification in contrast to the bulk traps. Furthermore, contrary to the literature that the trap states will accelerate the interface recombination, it is found that the interface electron recombination time is prolonged with Ce^{4+} surface traps in TiO_2 and Ti^{4+} bulk traps in SnO_2, indicating that the recombination time is closely related to the property of the trap states.

1. Introduction

Photoelectrochemical DSSC is attracting more and more attention due to its low cost and improving efficiency [1–3]. As an important part in DSSCs, porous wide-band gap semiconductor photoanodes take part in accepting and transporting the electrons from the adsorbed dye molecules [4]. Therefore, the electronic structure of the semiconductors (the conduction band potential, the trap states distribution) largely influences the electron transport in the porous electrode and the electron recombination process from photoanode to the redox couple. In order to tailor the property of the photoanode, several methods have been developed, one of which is the surface modification of a layer of wide band gap metal oxide, such as $SrTiO_3$ [5], MgO [6], ZnO [7] and Nb_2O_5 [8] on the porous photoanode. The purpose is to bring up the conduction band to negative potential and diminishment of the surface trap states and the interface recombination. The photovoltage is thus

* Corresponding author. Tel.: +86 0574 87600770; fax: +86 0574 87600744.
** Corresponding authors.
E-mail addresses: zhangjing@nbu.edu.cn (J. Zhang), zhuyuejin@nbu.edu.cn (Y. Zhu), HAN.liyuan@nims.go.jp (L. Han).

http://dx.doi.org/10.1016/j.jpowsour.2014.01.086
0378-7753/

usually improved by this method. Another method is doping metal or non-metal atom into photoanodes to tailor their property. It has been reported intensively that many positive effects have been achieved by doping to improve the performance of photoanode in DSSCs. Nb^{5+} (< 2% molar content) doping in TiO_2 effectively controlled the surface states, thus it facilitated the electron transport in TiO_2 photoanode [9,10]. W^{6+} doping in TiO_2 (within a 0.1–2% content) brought down the conduction band potential of photoanode, thus enlarged the driving force of the electron injection from the dye into the photoanode [11]. Zn^{2+} (< 0.7% content) doping in TiO_2 reduced the trap states of the nanocrystalline, which lead to the improvement of the electron transport [12]. It is noticed that the performance of the DSSCs does increase at a certain percentage of doping. However, it usually turns to decrease noticeably at higher doping amount with the reason unspecified or simply ascribed to the induced trap states which impede the electron transport. Though the negative role of the excessive trap states is assured, the type of trap states (whether it is a bulk or a surface trap state) and the effect of each trap states on the electron transport have not been discussed yet in the previous doping works.

The electron transport in photoanodes of DSSCs can be regarded as a trap–detrap electron diffusion process [13]. The trap states of pure nanocrystalline photoanode are mainly composed of surface trap states, because of the large surface area of the nanoporous films [14,15]. However, when a third element is doped in the nanocrystalline, it is prone to reside in the particle (substitute the lattice atoms or stay interstitial in the lattice) or on the surface of the nanocrystalline, thus forming bulk and surface trap states, respectively. Both the surface and bulk trap states influence the electron transport in DSSCs, while the surface states are usually considered as the interface recombination centers [14–17]. It is quite important to distinguish the surface trap states from bulk trap states in doping works, because they contribute differently to the electron transport of the photoanode and the methods to eliminate the trap states may be differed from each the other either. In our previous work, Ce^{4+} doped TiO_2 and Ti^{4+} incorporated SnO_2 photoanodes are prepared for DSSCs [18,19]. The performances of the DSSCs decrease at high amount of the added elements which is due to the excessive trap states formed. In this work, a comparison is carried out between Ce^{4+} doped TiO_2 photoanode and Ti^{4+} incorporated SnO_2 photoanode: the lattice structure and the chemical bonding of the nanocrystallines change differently with the third element amount increase, and the performances of the DSSCs respond differently with $TiCl_4$ surface treating of the electrode. According to the phenomenon, the type of trap states in Ce^{4+} doped TiO_2 and Ti^{4+} incorporated SnO_2 is assigned to surface traps and surface-and-bulk coexisted traps, respectively. The role of each trap states on the electron transport in the photoanodes and the special property of the trap states in the interface recombination process are discussed. It is suggested from the electron transport analysis that bulk trap states should be avoided during photoanode preparation to get high quality photoanodes of DSSCs.

2. Experimental section

2.1. Preparation of the photoanodes and DSSCs

Ce^{4+} doped TiO_2 and Ti^{4+} incorporated SnO_2 were prepared according to the literature [18,19]. The contents we discussed here were 0.3, 0.6 and 0.9% of Ce^{4+} doping, which were marked as Ce-03, Ce-06 and Ce-09, respectively; and 15, 40 and 70% of Ti^{4+} incorporated SnO_2 were marked as T15, T40 and T70 respectively. The photoanodes were prepared by screen printing the paste. After annealing at 500 °C for 30 min, the 0.25 cm^2 photoanodes were obtained. For $TiCl_4$ treatment, the photoanodes were immersed in $TiCl_4$ aqueous solution (40 mM) for 30 min at 70 °C. After washing by pure water and ethanol twice, the photoanodes suffered thermal treatment at 500 °C for 15 min again.

The prepared photoanodes were immersed in dye N719 solution (0.3 mM in acetonitrile and tertbutyl alcohol with volume ratio of 1:1) over night. The photoanode was sealed with Pt counter electrode by Surlyn films. The electrolyte (0.6 M methylpropylimidazolium iodide, 0.05 M I_2, and 0.1 M LiI in acetonitrile with tert-butyl pyridine) was back filled in the cell.

2.2. Characterization of the photoanodes

The X-ray diffraction (XRD, 20–60°) was performed by Rint-2500 diffractometer (Rigaku, Japan) with Cu Kα radiation operated at 40 kV and 300 mA. The incorporation of the elements in nanocrystal was examined by X-ray photoelectron spectroscopy (XPS, PHI Quantera SXM, Japan) using Al Kα radiation. The cyclic voltammetry (*CV*) was performed with the three electrodes system, using Pt wire as counter electrode, saturated calomel electrode (SCE) as reference electrode and the photoanode (thickness: 5 μm and area of 0.25 cm^2) as working electrode. 0.1 M $TBAPF_6$ (Tetrabutylammonium hexafluorophosphate) in acetonitrile was served as the supporting electrolyte.

2.3. *I–V* curves of the DSSCs and photoelectrochemical measurements

I–V curves of the DSSCs (active area of 0.2304 cm^2 by a black mask) were measured with a digital source meter (Keithley2400) under simulated solar illumination at 1 Sun, AM1.5 (Wacom, Japan). The intensity modulated photocurrent spectroscopy (IMPS) measurements were carried out on electrochemical work station (Solartron 1287 and 1255B) with two-electrode system under a series of light illumination (provided by 446 nm laser). The open circuit voltage decay (OCVD) spectra were also recorded by electrochemical work station after the simulated sunlight was turned off.

3. Results and discussions

3.1. Crystallinity change of the photoanodes by doping

Fig. 1 is the XRD patterns of Ce^{4+} doped TiO_2 and Ti^{4+} incorporated SnO_2 nanoparticles. Contrary to the similar peak position of Ce^{4+} doped TiO_2 photoanodes, the position of the diffraction

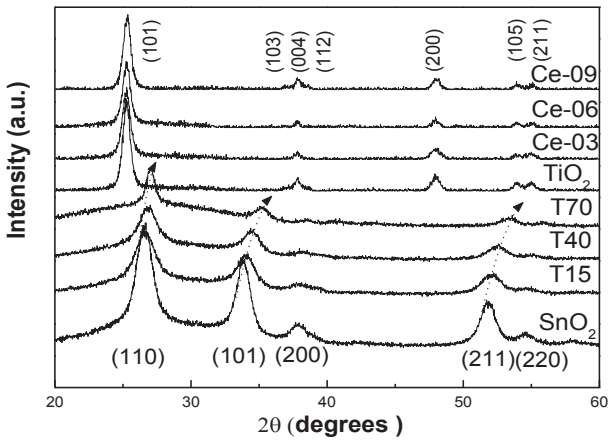

Fig. 1. XRD patterns of Ce^{4+} doped TiO_2 and Ti^{4+} incorporated SnO_2 photoanodes.

peak of Ti^{4+} incorporated SnO_2 nanoparticles moves obviously to high degree with increasing the Ti amount. It indicates the crystalline structure changes a lot with Ti^{4+} incorporated SnO_2, while keeps almost unchanged with Ce^{4+} doped TiO_2. Table 1 lists the lattice parameters of Ce^{4+} doped TiO_2 and Ti^{4+} incorporated SnO_2 samples, which are obtained from the Bragg function. The lattice parameters of Ce^{4+} almost did not change, however, the Ti^{4+} incorporated SnO_2 show the lattice shrinkage with increasing Ti content, which indicates that the Ti incorporation effectively changes the crystalline structure. The influence of doping atom to the crystalline structure is closely related to the incorporation situation of the doped atom and the size of doping element. The ionic radius of Ce^{4+} is 0.93 Å, which is much larger than the Ti^{4+} (0.68 Å) [20]. The mismatch of the two elements makes the Ce^{4+} hard to substitute Ti^{4+} in the lattice. The unchanged lattice parameters indicate that the Ce^{4+} unsuccessfully incorporated into the crystal lattice of TiO_2. If the Ce^{4+} unsuccessfully incorporated into the TiO_2 lattice, it is inclined to stay at the particle surface or the grain boundaries when the Ce content increase. By contrast, Ti^{4+} incorporated into the SnO_2 lattice obviously for the change of the lattice parameters. It formed $Ti_xSn_{1-x}O_2$ solid solution nanoparticles for the similar ionic radius of Ti^{4+} (0.68 Å) and Sn^{4+} (0.71 Å) and the close lattice parameters of tetragonal rutile SnO_2 and TiO_2 [21]. The Ti^{4+} can successfully substitute the Sn^{4+} in the lattice. For the smaller size of Ti^{4+} compared with Sn^{4+}, the lattice size shrinks with Ti^{4+} amount increase as Table 1 indicated.

Compared with the size of pure TiO_2 nanocrystalline in Table 1, the crystalline size of Ce^{4+} doped TiO_2 is decreased. The decreased crystalline size is also an evidence that Ce^{4+} is prone to stay at grain boundary or particle surface of TiO_2, because the Ce^{4+} at that site will inhibit the crystalline growth of TiO_2 [20]. The increased crystalline size of Ti incorporated SnO_2 in Table 1 indicates that Ti^{4+} is easy to participate in and promote the crystallization process. The Ti^{4+} can reside both on the surface and in the lattice of the SnO_2 nanocrystalline.

TEM images of Ce^{4+} doped TiO_2 and Ti^{4+} incorporated SnO_2 (Fig. 2) clearly show the morphologies of the nanocrystalline and the lattice structure of the samples. The TEM results are consistent with the lattice parameters obtained from the XRD results: the crystalline size of TiO_2 is a little decreased with Ce^{4+} (0.9%) doping, while the size of T70 is much larger than the pure SnO_2. On the other hand, the distance of lattice plane of Ce-09 is almost unchanged compared with TiO_2, while incorporation of Ti in SnO_2 clearly shrinks the lattice plane distance when compared with SnO_2.

The lattice structure and size change of doped nanocrystallines indicates that the Ti is prone to participate in the crystalline growth of $Ti_xSn_{1-x}O_2$, thus change the crystalline structure greatly. However, the Ce^{4+} is unreactive to enter in the lattice of TiO_2 to influence the crystalline growth.

Table 1
The lattice cell parameters and the crystalline size of the nanoparticles.

Sample	Lattice cell parameter (Å)		Average crystalline size (nm)
	a	*c*	
Ce-0	3.789	9.498	13.07
Ce-03	3.787	9.532	12.16
Ce-06	3.787	9.509	12.68
Ce-09	3.786	9.513	12.25
SnO_2	4.722	3.199	7.20
T15	4.730	3.149	8.79
T40	4.671	3.117	9.61
T70	4.653	3.034	12.26

3.2. XPS of the Ce^{4+} doped TiO_2 and Ti^{4+} incorporated SnO_2

XPS in Fig. 3 indicates the chemical bonding situation of the doped nanocrystallines. In XPS plots of Ce^{4+} doped TiO_2 (Fig. 3a–c), there is no obvious shift of the Ti 2p and O 1s bonding, indicating the chemical bonding is not changed by Ce^{4+} doping. At the same time, there exists the Ce 3d 3/2 and Ce 3d 5/2 peaks at around 885 and 905 eV, which implies the co-existence of both Ce^{3+} and Ce^{4+} oxidation states [18,20]. For the Ce^{4+} incorporation does not change the binding energy of the nanocrystalline, it is deduced that the Ce is inclined to stay outside the nanocrystalline. In XPS of Ti^{4+} incorporated SnO_2 nanoparticles (Fig. 3d–f), the chemical bonding of the elements changed a lot by Ti^{4+} incorporation for the peaks of Sn 3d, O 1s and Ti 2p peaks move to lower binding energy with increasing the Ti^{4+} content. The decrease of the binding energy indicates the Ti^{4+} enters and induces distortion of the lattice, which will weaken the bonding of the elements and induce oxygen deficiency in the nanocrystalline [22].

3.3. Performances of the DSSCs with photoanodes before and after $TiCl_4$ treating

Fig. 4 is the *J–V* curves of DSSCs with Ce doped TiO_2 and $Ti_xSn_{1-x}O_2$ photoanodes. The performances of DSSCs with photoanodes after $TiCl_4$ treatment are also indicated. The detailed photovoltaic parameters are listed in Table 2. With increasing the Ce amount from 0.3% to 0.9%, the performance consistently decreases from 6.0% to 3.78%. Compared with the performance 6.41% of the undoped DSSC, the performances of Ce 0.6% and 0.9% doped DSSCs decrease by about 15.9% and 41% respectively. It is noticed that the loss of J_{sc} is the main reason of the decreased performance. J_{sc} is proportional to the electron injection efficiency (η_{inj}) of the dye to photoanode, the light harvest efficiency (η_{lh}) and the electron collection efficiency (η_{cc}) of the photoanode [23]. For the unchanged transparency and the dye adsorption amount of the Ce^{4+} doped photoanodes, the η_{lh} and η_{inj} are not the reason for the impaired J_{sc}. The excessive traps states which impede the electron transport in the photoanode may reduce the η_{cc}, thus bring down the J_{sc} [18]. Interestingly, it is found that the performances of DSSCs with Ce-03, Ce-06 and Ce-09 photoanodes are largely recovered to 7.31%, 7.28% and 6.64% respectively by $TiCl_4$ treatment, which can even compete with the 7.2% of the undoped DSSCs with $TiCl_4$ treating. Generally, there is a 30 mV improvement of V_{oc} after $TiCl_4$ treatment for all the samples which is due to that the increased dye adsorption of the photoanode and the reduced interface recombination by $TiCl_4$ treating enlarge the energy difference (V_{oc}) between photoanodes and redox electrolyte [24,25]. Obviously, the J_{sc} of DSSCs with Ce-03, Ce-06 and Ce-09 photoanodes is largely increased by $TiCl_4$ surface treatment. The dye adsorption of $TiCl_4$ treated photoanodes are almost the same in Table 2, therefore it is the η_{cc} which is recovered by the surface treating of Ce-03, Ce-06 and Ce-09 improves the J_{sc}.

The performances of DSSCs with $Ti_xSn_{1-x}O_2$ photoanodes with and without $TiCl_4$ treatment are indicated in Fig. 4b and Table 2. Obviously, with Ti incorporation, the V_{oc} increases, however, J_{sc} decreases largely. With 40% Ti incorporated in, the performance of the DSSC even decreases to 0.137%. The improved V_{oc} is related to the negative movement of conduction band position, while the decreased J_{sc} is ascribed to the impaired electron transport in the photoanode by the induced trap states [19]. After $TiCl_4$ treatment, the DSSC with SnO_2 photoanode shows increase of the performance of more than 3 times. By contrast to the recovered performance of DSSCs with $TiCl_4$ treated Ce doped TiO_2 photoanodes, the performances of DSSCs with $TiCl_4$ treated T40 and T70 photoanodes do

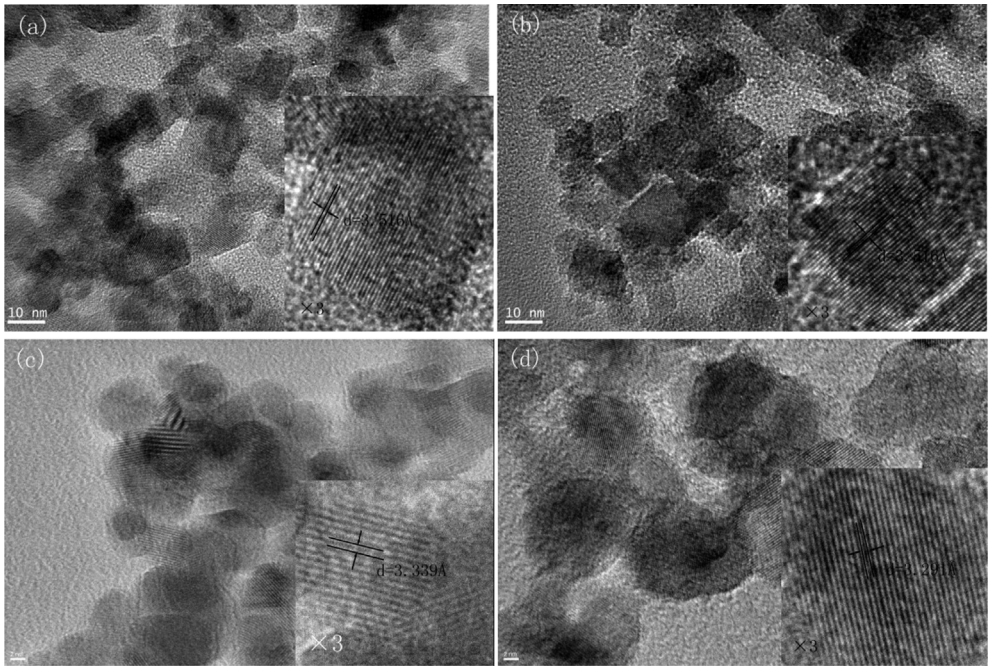

Fig. 2. TEM images of TiO_2 (a), Ce-09 (b), SnO_2 (c) and T70 (d). The insert of each picture is the magnified image (magnification of 3) and the lattice distance *d* is indicated.

not recover to the level of DSSC with $TiCl_4$ treated SnO_2 photoanode. The performances are improved to 3.76%, 2.41% and 2.9% of DSSCs with $TiCl_4$ treated T15, T40 and T70, respectively, which are far behind the 4.17% of DSSC with $TiCl_4$ treated SnO_2. It is clear that J_{sc} (electron collection efficiency η_{cc}) of T15, T40 and T70 cannot be recovered by $TiCl_4$ surface treatment.

Both of the two kinds of photoanodes show impaired J_{sc} with the added elements amount increase and the reason is ascribed to the excessive trap states. However, the two kinds of photoanodes respond differently after $TiCl_4$ surface modification which is due to the position of the trap states is different.

3.4. CV curves of the photoanodes and its implications to the trap states distribution

Fig. 5a shows the *CV* curves of the different Ce amounts doped TiO_2 photoanodes and Fig. 5b is the curves of the $TiCl_4$ treated photoanodes. A cathodic peak as the arrow indicated in the *CV* curves of the Ce-03, Ce-06 and Ce-09 photoanodes is assigned to the reduction of Ce^{4+} to Ce^{3+} in the samples [26]. The change of Ce^{4+} to Ce^{3+} is an electron trap process that deteriorates the electron transport. Obviously, the cathodic peaks in *CV* curves of Ce-03, Ce-06 and Ce-09 disappear after $TiCl_4$ treatment. $TiCl_4$ is a

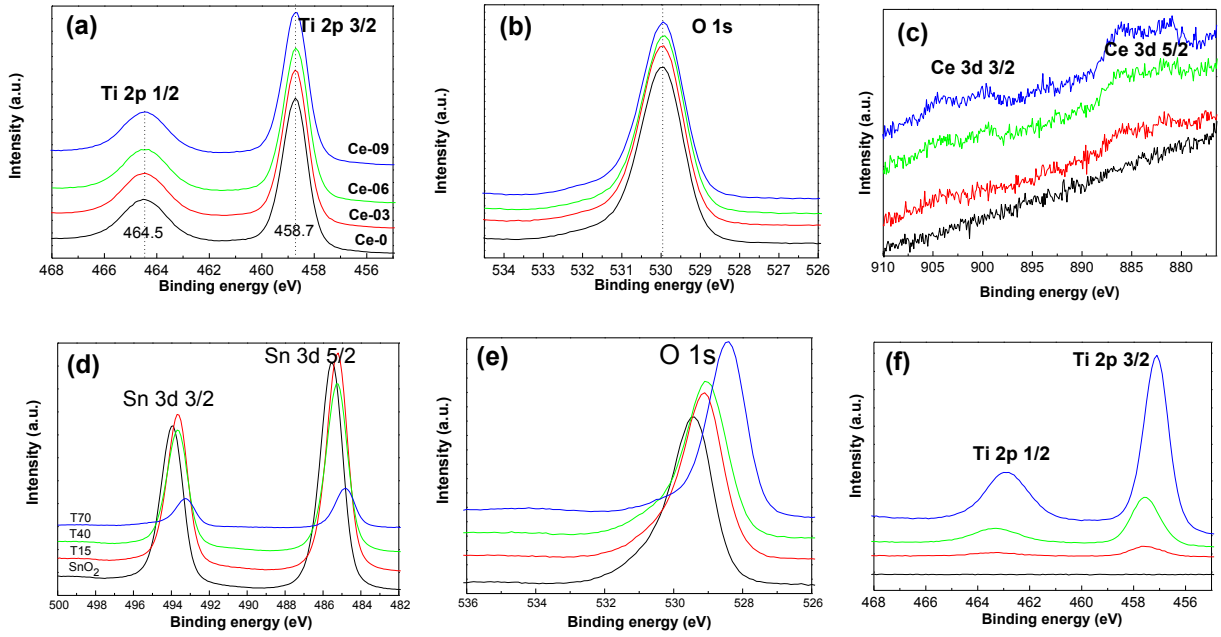

Fig. 3. XPS plots of Ce doped TiO_2: Ti 2p (a), O 1s (b), Ce 3d (c); Ti incorporated SnO_2: Sn 3d (d), O 1s (e) and Ti 2p (f).

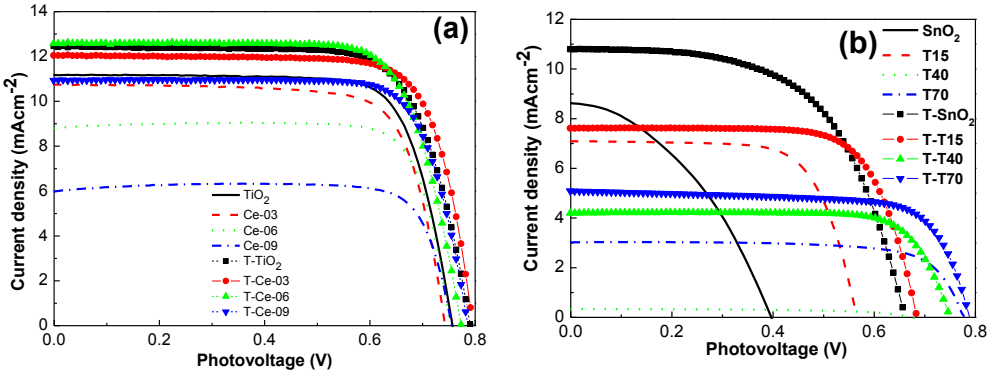

Fig. 4. The *J*–*V* curves of DSSCs with Ce doped TiO_2 (a) and $Ti_xSn_{1-x}O_2$ (b) photoanodes (the DSSCs with $TiCl_4$ treatment is noted as T-series).

surface treatment on TiO_2 photoanode that is reported to increase the surface area, improve the electron injection and suppress the interface recombination of the DSSCs [24,25]. Thus, $TiCl_4$ modification on the Ce doped TiO_2 photoanodes passivates the trap states induced by Ce^{4+}. Considering $TiCl_4$ is a surface treatment which effectively eliminates the Ce^{4+} trap states, it is deduced that the Ce^{4+} mostly reside on the surface of the photoanode, serving as surface trap states that influence the electron transport. It is the reason that the performance of DSSCs sharply decreases with small Ce^{4+} amount doped photoanodes. After the $TiCl_4$ modification, most of the surface states are passivated; therefore the performances of the DSSCs with Ti doped photoanodes catch up with the undoped one.

In XRD and XPS results, with increase the Ce^{4+} in TiO_2, there is no clear change of the lattice parameters of TiO_2 and the chemical bonding the elements, implying that the large size of Ce^{4+} may be unsuccessfully incorporated into the TiO_2 lattice, but reside on the surface of the nanocrystalline. Thus, the surface property of TiO_2 may change a lot by $TiCl_4$ treating as *CV* indicated. By contrast, with increase of Ti^{4+} in SnO_2, the lattice parameters and the chemical binding change regularly. The formation of $Ti_xSn_{1-x}O_2$ indicates that Ti successfully substitutes Sn in the lattice. Thus, both the surface and inert property of $Ti_xSn_{1-x}O_2$ may be quite different from pure SnO_2.

Fig. 6a is the *CV* curves of $Ti_xSn_{1-x}O_2$ photoanodes. With Ti incorporation amount increase, the onset current position moves gradually to negative potential when applying the negative scan. It indicates that the conduction band potential negatively changes with Ti amount increase. The potential is changed from 0.2 V (vs. SCE) of SnO_2 to −0.05 V of T15, −0.13 V of T40 and −0.3 V of T70, which is in accordance with the V_{oc} change. The other phenomenon is that the current density of the *CV* curve during cathodic scan decreased a lot with increasing the Ti incorporation amount. The cathodic current density is proportional to the capacitance of the photoanode according to the equation [27]:

$$I = dQ/dt = CdV/dt \quad (1)$$

where *C* is the capacitance of the photoanode, dV/dt is the scan rate of the *CV* curve. The decreased current density of Ti incorporated photoanodes indicates that the capacitance of the films suffers loss. It is concluded that the capacitance which is corresponds to the electron accumulation ability of the photoanode [28] decreases after Ti is incorporated in the film. The decreased electron accumulation ability means fewer electrons can reside or transport in the photoanode, thus, leads to the deteriorated performance of the DSSCs.

After the $TiCl_4$ treating, the *CV* curves are quite different from the untreated ones. Firstly, the onset potential of the cathodic current negatively moves to 0.05, −0.13 and −0.21 V (vs. SCE) of the $TiCl_4$ treated SnO_2, T15 and T40 respectively, compared with the untreated ones. Together with the dye adsorption amount increase, the negative movement of the conduction band ascribes to the increase of V_{oc} after $TiCl_4$ modification. Secondly, the pattern of the *CV* curves changes a lot after $TiCl_4$ modification. A cathodic peak of SnO_2 photoanode which might be due to the reduction of the surface states of the SnO_2 photoanode disappears after $TiCl_4$ modification. It leads to the performance increase of the DSSC with SnO_2 after $TiCl_4$ modification. The *CV* curves of $TiCl_4$ treated T15, T40 and T70 enlarge a lot compared with untreated ones, which indicates the electron accumulation ability of the films enhances after $TiCl_4$ modification. However, the cathodic current density of *CV* patterns of the $TiCl_4$ treated T15, T40 and T70 photoanodes cannot catch up with the value of the SnO_2 photoanode, which implies that the electron accumulation/transport property of T15, T40 and T70 photoanodes cannot be recovered by $TiCl_4$ modification. Considering $TiCl_4$ treatment is a surface modification, it is concluded that a portion of trap states of T15, T40 and T70 is bulk trap states that cannot be passivated by the surface modification. The hard-to-removed bulk trap states of T15, T40 and T70 impede the electron transport in the photoanodes of DSSCs which leads to the uncorrectable performances of the DSSCs.

Table 2
The photovoltaic parameters of the DSSCs and the dye adsorption amount (DA) of the photoanode. T-sample is the $TiCl_4$ treated photoanode.

	J_{sc} [mA cm^{-2}]	V_{oc} [V]	F.F.	Eff [%]	DA (10^{-7} mol cm^{-2})
TiO_2	11.2	0.757	0.758	6.41	1.39
T–TiO_2	12.5	0.791	0.730	7.20	1.63
Ce-03	10.7	0.743	0.751	6.00	1.42
T–Ce-03	12.0	0.795	0.763	7.31	1.70
Ce-06	8.80	0.753	0.814	5.39	1.39
T–Ce-06	12.6	0.773	0.749	7.28	1.70
Ce-09	5.98	0.756	0.837	3.78	1.31
T–Ce-09	10.9	0.786	0.772	6.64	1.65
SnO_2	8.63	0.397	0.40	1.37	0.55
T–SnO_2	10.8	0.661	0.585	4.17	0.96
T15	7.09	0.566	0.698	2.80	0.72
T–T15	7.61	0.685	0.721	3.76	1.0
T40	0.336	0.673	0.605	0.137	0.79
T–T40	4.2	0.750	0.767	2.41	1.1
T70	3.02	0.776	0.731	1.71	0.74
T–T70	5.09	0.788	0.723	2.90	1.1

3.5. The electron transport ability of the DSSCs with two kinds of the photoanodes

From the *CV* analysis, it is concluded that the Ce^{4+} states mostly reside on the surface of TiO_2 photoanode and can be passivated by

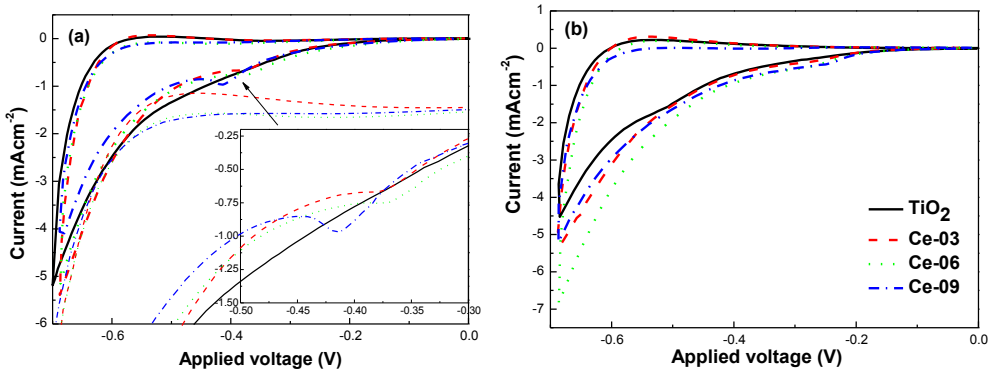

Fig. 5. The *CV* curves of the different Ce amounts doped TiO_2 photoanodes before (a) and after (b) $TiCl_4$ treatment.

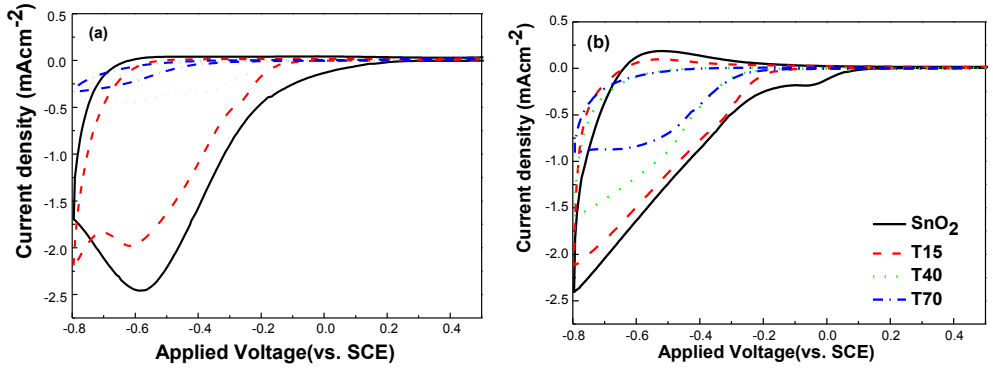

Fig. 6. The *CV* curves of $Ti_xSn_{1-x}O_2$ photoanodes before (a) and after (b) $TiCl_4$ treatment.

$TiCl_4$ modification; by contrast, a part of the Ti^{4+} may reside in the crystalline of the SnO_2, acting as the bulk trap states which cannot be recovered by the surface modification method. The electron transport property of the photoanodes is further characterized by IMPS method. The electron transport in the porous photoanodes of DSSCs is accepted as a diffusion process with electrons trap–detrap from the trap states and diffuse to the conducting glass [13]. Electron diffusion coefficient D_n which is calculated from the response time of the IMPS depicts the electron transport property of the photoanodes.

Fig. 7a is the D_n values of the Ce doped photoanodes with and without $TiCl_4$ treatment. With Ce doping, the electron transport time is prolonged by the induced Ce^{4+} trap states, thus, the D_n is decreased. However, the electron transport property is largely improved by $TiCl_4$ surface treatment, especially for the Ce doped photoanodes. It verifies that Ce^{4+} which is a surface trap state deteriorates the electron transport and can be recovered by surface treatment.

In Fig. 7b, the D_n value of T40 photoanodes decreases to the lowest, compared with other photoanodes. It is also the reason of the worst performance of DSSC with T40 photoanode. T70 shows higher D_n and performance than that of T40, which might be more Ti–O chemical bonds are formed in T70 that facilitates the electron transport. D_n does not recover after $TiCl_4$ modification, especially for the T40 photoanode. Thus, it is concluded that T40 have the most trap states, especially the bulk trap states. It verifies that the bulk trap states cannot be passivated by surface treatment, so that they impede the electron transport and deteriorate the performance of the DSSC.

Except for works on improving the light harvest efficiency (η_{lh}) [29,30] and electron injection efficiency (η_{inj}) [10,11,31] of the photoanodes, there are many contributions on nanoparticles with well-designed crystallinity [32,33], thus the charge collection

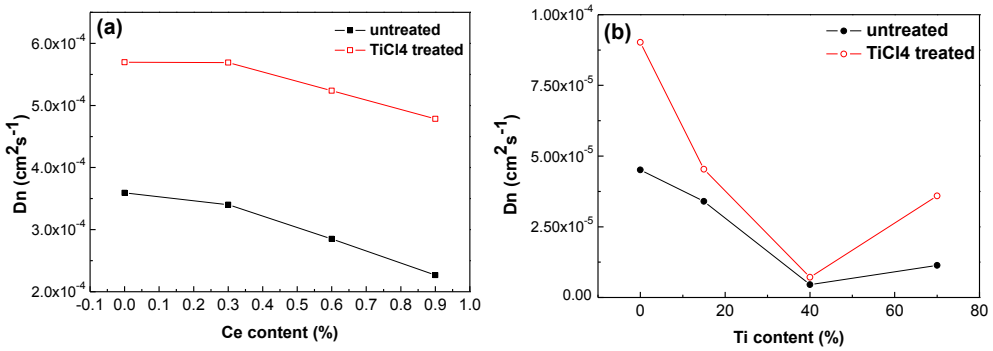

Fig. 7. The D_n values of the Ce doped TiO_2 photoanodes (a) and Ti incorporated SnO_2 photoanodes (b) with and without $TiCl_4$ treatment.

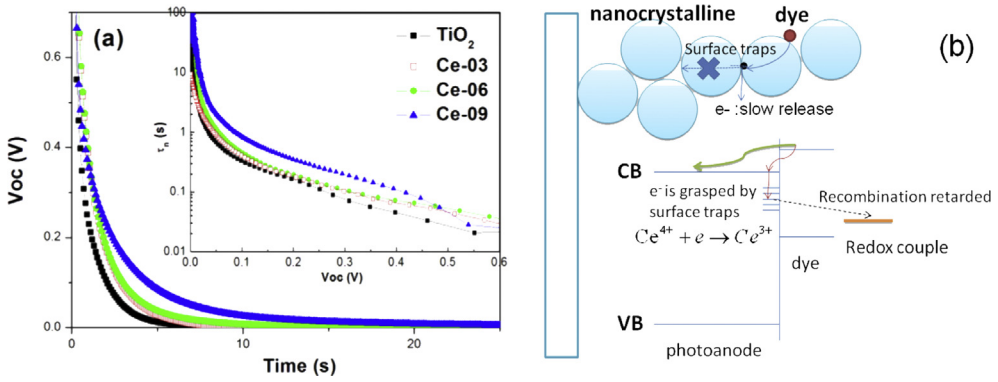

Fig. 8. The photovoltage decay of the DSSCs with Ce doped TiO_2 photoanodes (a), the electron response time with V_{oc} is plotted in the inset of figure; the scheme of electron transport and interface recombination of Ce^{4+} doped TiO_2 (b).

efficiency (η_{cc})/electron transport property of the photoanodes are superior to the common 20–30 nm nanoparticles. Excellent J_{sc} and performance of the DSSCs are achieved. It indicates that the well crystallized nanoparticles without bulk traps are benefit for the η_{cc}. Therefore, bulk trap states should be avoided in the nanocrystalline fabrication process for they are hard to remove and impair the J_{sc} of the DSSCs.

3.6. Interface electron recombination properties of photoanodes with different traps

Both Ce^{4+} surface and Ti^{4+} induced bulk trap states of excessive amount deteriorate the electron diffusion in the photoanodes from the above discussions. It is widely accepted that the interface electron recombination is mainly from the surface states of the photoanode to the redox couple [16]. The electrons in the bulk traps only exchange with the conduction band, then finally discharged from the semiconductor through the surface traps and recombine with the redox electrolyte [34]. In the OCVD experiments of DSSCs, the electron recombination properties of the two kinds of photoanodes are checked. The decay of photovoltage of the DSSCs is presented in Figs. 8a and 9a. The response time of the electrons from photoanode to the redox electrolyte which indicated in the inset of figure is obtained by Ref. [34]:

$$\tau_n = -\frac{k_B T}{e}\left(\frac{dV_{oc}}{dt}\right)^{-1} \quad (2)$$

Contrary to the reported references that the surface trap states of the photoanodes (usually Ti^{3+} surface states [35]) will accelerate the interface recombination and decrease the electron lifetime [34], the electron response time is prolonged by Ce^{4+} surface states in Fig. 8a, indicating the interface recombination is retarded. The reduction of the interface recombination time is ascribed to its special redox property of $Ce^{4+} + e \rightarrow Ce^{3+}$: Ce^{4+} grasps the electrons and prohibits the electron back transport [18,26]. That is the reason of the superior FF of Ce doped photoanode than the undoped one as Table 2 indicated. The scheme of electron transport in DSSC with Ce surface traps is presented in Fig. 8b.

It is clear that the shape of the curves differs in Fig. 9a. The electron response time is largely improved by T15, compared with DSSC with pure SnO_2. It indicates that the interface recombination is effectively reduced. The curve of response time τ_n with V_{oc}, the linearly increase of τ_n in low V_{oc} region is controlled mainly by bulk trap states, while the inverted parabolic curve at low V_{oc} is dominated by surface states [34]. Thus, for the heavy amount of Ti states in $Ti_xSn_{1-x}O_2$, the trap states in T40 are mainly the bulk traps, whereas T70 mainly exhibits surface traps. The conclusion is in accordance with the above electron transport ability tests that the bulk trap states in T40 is hard to remove, so that the performance of DSSC with T40 becomes the worst, even with the $TiCl_4$ surface modification. The insert plot of Fig. 9a also shows that the response time is prolonged by DSSC with T40, compared to that with pure SnO_2. The quick trapping and slow releasing the electrons from the bulk traps makes the recombination time long [36]. However, DSSC with T70 shows sharp decrease of the response time, which might be due to the easy leakage of the electrons from the surface trap states. The scheme of the function of bulk trap states is shown in Fig. 9b.

From the OCVD measurements, it is found that the electron response time is prolonged in the Ce^{4+} doped TiO_2 photoanodes

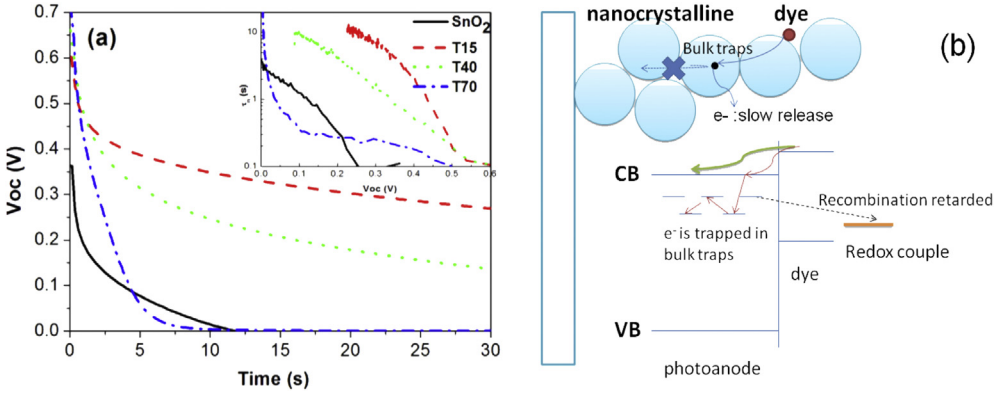

Fig. 9. The photovoltage decay of the DSSCs with Ti incorporated SnO_2 photoanodes (a), the insert is the electron response time with V_{oc}; the scheme of electron transport and interface recombination of DSSC with bulk traps (b).

and T40 photoanode, which is due to the special property of each trap states. However, the total electron recombination amount is considered to increase of the photoanodes with the trap states. Because the trapped electrons in the photoanodes will not transport to the outer circuit and finally discharge from the trap states to recombine with the redox electrolyte [34].

4. Conclusions

From the crystallinity, XPS characterizations and the performances of Ce^{4+} doped TiO_2 photoanode and Ti^{4+} incorporated SnO_2 photoanode with and without $TiCl_4$ treatment, two different kinds of trap states (surface and bulk trap states) are assigned: Ce^{4+} acts as surface trap states on the TiO_2 nanocrystallines, while Ti^{4+} resides both on the surface and in the bulk of the SnO_2 nanocrystallines.

From the *CV* analysis and electron transport property of the photoanodes before and after $TiCl_4$ treatment, it is concluded that: both the surface and bulk trap states deteriorate the electron transport in the photoanodes, however, it is found that the surface trap states can be removed by the surface modification, while the bulk trap states cannot be easily passivated. So the bulk trap states should be avoided during the photoanode preparation to realize the high performance of the DSSCs. Furthermore, DSSCs with Ce-06, Ce-09 and T40 photoanodes show prolonged electron response time of recombination compared with the undoped DSSCs, which might be due to the trap states grasp the electrons and retard the interface electron recombination.

Acknowledgment

The authors acknowledge the financial support from the National Natural Science Foundation of China (Grant No. 51302137, 11304170 and 11374168), Qiangjiang Talented Person Project of Zhengjiang (No. QJD1302008) and K.C. Wong Magna Fund in Ningbo University.

References

[1] B. O'Regan, M. Grätzel, Nature 353 (6346) (1991) 737–740.
[2] L. Han, et al., Energy Environ. Sci. 5 (3) (2012) 6057–6060.
[3] A. Yella, et al., Science 334 (6056) (2011) 629–634.
[4] M. Grätzel, J. Photochem. Photobiol. C Photochem. Rev. 4 (2) (2003) 145–153.
[5] Y. Diamant, et al., J. Phys. Chem. B 107 (9) (2003) 1977–1981.
[6] H.S. Jung, et al., Langmuir 21 (23) (2005) 10332–10335.
[7] S.J. Wu, et al., Appl. Phys. Lett. 92 (12) (2008).
[8] S.G. Chen, et al., Chem. Mater. 13 (12) (2001) 4629–4634.
[9] T. Nikolay, et al., Energy Environ. Sci. 4 (4) (2011) 1480–1486.
[10] X. Lü, et al., Adv. Funct. Mater. 20 (3) (2010) 509–515.
[11] X. Zhang, et al., J. Phys. Chem. C 115 (25) (2011) 12665–12671.
[12] K.P. Wang, H. Teng, Phys. Chem. Chem. Phys. 11 (41) (2009) 9489–9496.
[13] A.J. Frank, N. Kopidakis, J.V.D. Lagemaat, Coord. Chem. Rev. 248 (13–14) (2004) 1165–1179.
[14] J. van de Lagemaat, A.J. Frank, J. Phys. Chem. B 104 (18) (2000) 4292–4294.
[15] D. Cahen, et al., J. Phys. Chem. B 104 (9) (2000) 2053–2059.
[16] G. Schlichthörl, et al., J. Phys. Chem. B 101 (41) (1997) 8141–8155.
[17] F. Fabregat-Santiago, et al., J. Appl. Phys. 96 (11) (2004) 6903–6907.
[18] J. Zhang, et al., J. Phys. Chem. C 116 (36) (2012) 19182–19190.
[19] J. Zhang, et al., J. Mater. Chem. A 1 (29) (2013) 8453–8463.
[20] Y. Zhang, et al., J. Phys. Chem. C 113 (51) (2009) 21406–21412.
[21] L. Trotochaud, S.W. Boettcher, Chem. Mater. 23 (22) (2011) 4920–4930.
[22] X. Dou, et al., Chem. Mater. 23 (17) (2011) 3938–3945.
[23] Y. Tachibana, et al., Chem. Mater. 14 (6) (2002) 2527–2535.
[24] B.C. O'Regan, et al., J. Phys. Chem. C 111 (37) (2007) 14001–14010.
[25] P.M. Sommeling, et al., J. Phys. Chem. B 110 (39) (2006) 19191–19197.
[26] K.L. Frindell, et al., Chem. Mater. 16 (18) (2004) 3524–3532.
[27] F. Fabregat-Santiago, et al., J. Phys. Chem. B 107 (3) (2002) 758–768.
[28] J. Bisquert, V.S. Vikhrenko, J. Phys. Chem. B 108 (7) (2004) 2313–2322.
[29] D. Chen, et al., Adv. Mater. 21 (21) (2009) 2206–2210.
[30] W. Peng, L. Han, J. Mater. Chem. 22 (38) (2012) 20773–20777.
[31] J. Liu, et al., Electrochim. Acta 56 (1) (2010) 396–400.
[32] H.-P. Wu, et al., J. Phys. Chem. Lett. 4 (9) (2013) 1570–1577.
[33] J.-W. Shiu, et al., ACS Nano 6 (12) (2012) 10862–10873.
[34] J. Bisquert, et al., J. Am. Chem. Soc. 126 (41) (2004) 13550–13559.
[35] Y. Yu, K. Wu, D. Wang, Appl. Phys. Lett. 99 (19) (2011) 192104–192113.
[36] D. Zhao, et al., J. Phys. Chem. C (2008) 8486–8494.